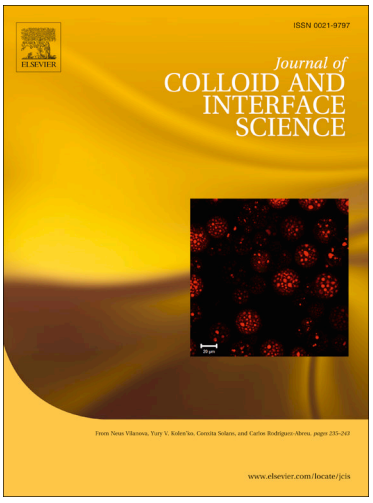

Phosphate removal from aqueous solution using iron oxides: adsorption, desorption and regeneration characteristics

Zeeshan Ajmal, Atif Muhmood, Muhammad Usman, Simon Kizito, Jiaxin Lu, Renjie Dong, Shubiao Wu

PII: S0021-9797(18)30603-9
DOI: https://doi.org/10.1016/j.jcis.2018.05.084
Reference: YJCIS 23662

To appear in: *Journal of Colloid and Interface Science*

Received Date: 14 March 2018
Revised Date: 22 May 2018
Accepted Date: 22 May 2018

Please cite this article as: Z. Ajmal, A. Muhmood, M. Usman, S. Kizito, J. Lu, R. Dong, S. Wu, Phosphate removal from aqueous solution using iron oxides: adsorption, desorption and regeneration characteristics, *Journal of Colloid and Interface Science* (2018), doi: https://doi.org/10.1016/j.jcis.2018.05.084

Phosphate removal from aqueous solution using iron oxides: adsorption, desorption and regeneration characteristics

Zeeshan Ajmal[a], Atif Muhmood[a], Muhammad Usman[b,c], Simon Kizito[ad], Jiaxin Lu[a], Renjie Dong[a], Shubiao Wu[ae]*,

[a] Key Laboratory of Clean Utilization Technology for Renewable Energy in Ministry of Agriculture, College of Engineering, China Agricultural University, Beijing, PR China.

[b] Environmental Mineralogy, Center for Applied Geosciences, University of Tübingen, 72074 Tübingen, Germany.

[c]Institute of Soil and Environmental Sciences, University of Agriculture, Faisalabad, 38040, Pakistan.

[d] College of Agricultural and Environmental Sciences, Makerere University, Uganda

[e]Aarhus Institute of Advanced Studies, Aarhus University, Høegh-Guldbergs Gade 6B, DK-8000 Aarhus C, Denmark

*Corresponding author. E-mail address: wushubiao@gmail.com

Abstract

Dynamics of phosphate (PO_4^{3-}) adsorption, desorption and regeneration characteristics of three lab-synthesized iron oxides, ferrihydrite (F), goethite (G), and magnetite (M) were evaluated in this study. Batch experiments were conducted to evaluate the impact of several adsorption parameters including adsorbent dosage, reaction time, temperature, pH, and ionic strength. The results showed that PO_4^{3-} adsorption increased with reaction time and temperature while it decreased with an increase in solution pH. Adsorption isotherm data exhibited good agreement with the Freundlich and Langmuir model with maximum monolayer adsorption capacities of 66.6 $mg \cdot g^{-1}$ (F), 57.8 $mg \cdot g^{-1}$ (M), and 50.5 $mg \cdot g^{-1}$ (G). A thermodynamics evaluation produced $\Delta G < 0$, $\Delta H > 0$, and $\Delta S > 0$, demonstrating that PO_4^{3-} adsorption onto tested minerals is endothermic, spontaneous, and disordered. The PO_4^{3-} removal mostly occurred via electrostatic attraction between the sorbate and sorbent surfaces. Moreover, the PO_4^{3-} sorption was reversible and could be desorbed at varying rates in both neutral and alkaline environments. The good desorption capacity has practical benefits for potential regeneration and re-use of the saturated particles in wastewater treatment systems.

Keywords

Phosphate; iron oxides particles; wastewater treatment; Regeneration.

1. Introduction

Phosphorus as orthophosphate (PO_4^{3-}) is an essential macronutrient in aquatic resources but its excessive supply through industrial, agricultural, and household activities leads to eutrophication in water bodies [1]. One way to achieve the regulation for controlling and reducing the eutrophication problem is to recover PO_4^{3-} in wastewater. Previously, various techniques have been successfully employed for PO_4^{3-} removal from wastewater. They include; chemical precipitation [2], biological treatment [3], struvite formation [4] membrane processing [5], and adsorption [6, 7]. Compared to the biological treatments, the chemical precipitation is a more effective technique for PO_4^{3-} removal. However, it

has a major setback where excessive chemical reagents and the accumulated sludge may cause secondary pollution [8]. Given that the biological process depends on phosphorus accumulating bacteria, the systems may not be easily optimized for PO_4^{3-} removal [9] and thus biological treatment cannot satisfy strict discharge requirements without further treatment [10].

Sorption processes often show good potential for removing PO_4^{3-} from contaminated water [11] by offering several advantages, such as low sludge production and simple operation [12]. However, the sorption efficiency is more dependent on the nature of adsorbent and reaction conditions. From literature several adsorbents have been investigated to remove PO_4^{3-} from wastewater and the most successful ones include; iron oxides [13], mesosilicates [14], zeolite [15], biochar [16], red mud [17], and aluminum oxides [18]. Moreover, there is an increased interest in the use of waste iron minerals for water treatment and phosphate recovery. Removal of PO_4^{3-} ions has been evaluated using different iron oxides, including ferrihydrite ($Fe(OH)_3$) where PO_4^{3-} adsorption reached 104.8 $mg \cdot g^{-1}$ at pH 4 [19] , magnetite (Fe_3O_4) [20] and goethite (α-FeOOH), at which PO_4^{3-} adsorption was found be most favorable with adsorption rate 10 $mg \cdot g^{-1}$ at low concentration 0.3 $mg \cdot L^{-1}$ [21], and green rust which showed highest adsorption capacity 64.1 $mg \cdot g^{-1}$ at pH 4 [22]. Removal of PO_4^{3-} has also been studied by magnetite seeded precipitation [23] and industrial waste iron oxide tailings [24].

Despite, the increasing evidence regarding high recovery of phosphate onto metal oxides, very limited data is available about the comparison of dynamic adsorption/desorption characteristics of PO_4^{3-} on different iron oxides and their regeneration for subsequent treatments. To address these knowledge gaps, further studies are required to compare the PO_4^{3-} removal by using iron oxides having different morphological and physicochemical properties. Therefore, the present study aimed at providing a detailed description of the desorption and regeneration mechanisms for the PO_4^{3-} adsorbed onto three different iron oxides including ferrihydrite (F), goethite (G), and magnetite (M). The influence of operational parameters, such as pH, reaction time, initial concentration, adsorbent dose, and temperature were examined. In addition, the adsorption behaviours of the tested adsorbents were evaluated by conducting both sorption kinetic and equilibrium isotherm

modelling. Finally, the potential applications of these materials were identified using desorption and regeneration capacities. For this purpose, seven adsorption/desorption cycles were performed in order to determine the potential applicability of regenerated particles by making their further implication as a monetary feasible strategy for PO_4^{3-} recovery.

2. Materials and Methods

2.1 Synthesis and characterization of iron oxides

The iron minerals namely; ferrihydrite [25], magnetite [26], goethite [27] were synthesized using already established methods. Their crystal structure was determined by using x-ray diffractometry (XRD, D8-Advance, Bruker Co., Japan) excited with Cu Kα radiation at 45 kV and 100 mA. Specific surface area was measured using the multipoint N_2 Brunauer–Emmett-Teller (BET) method (Quadrasorb SI MP) at 77 K. The primary particle size and morphology of the synthesized materials were examined using transmission electron microscopy (TEM; Hitachi 7700, Japan) at 100 kV. Surface and structural chemical functional groups were determined using Fourier-transform infrared (FTIR) spectroscopy (Varian Excalibur 3100). Scanning electron microscope coupled with energy dispersive X-ray spectrometry (EDX) analyses were conducted on an FEI XL.30 S-FEG SEM (USA). The point of zero charge (pzc) was measured following the method described in [28]. The total iron content was measured using inductively coupled plasma mass spectroscopy (ICP-MS; ICP-Nexion 300X, PerkinElmer USA).

2.2. Batch adsorption and desorption experiments

Batch adsorption studies were conducted using synthetic PO_4^{3-} solutions. A stock solution (1000 $mg \cdot L^{-1}$) was prepared using anhydrous potassium dihydrogen phosphate (KH_2PO_4; 99.5 %) and then diluted to the desired concentrations for further experimentation. Various experimental factors such as sorption time (0 – 480 min), sorbent dose (1 – 12 $g \cdot L^{-1}$), temperature (15 – 55 °C), initial PO_4^{3-} concentration (200 – 1000 $mg \cdot L^{-1}$), and ionic strength (0.0010 – 0.05 N) were studied at pH 7.0 ± 0.1. The pH was controlled using NaOH/HCl solutions. After sorption, all samples were centrifuged

at 8000 rpm for 10 min and their supernatant (10 mL) was filtered through 0.45 μm cellulose acetate membrane filters. Prior to analyses, the supernatant was acidified with 0.5M HNO_3 and stored in acid washed bottles. The residual PO_4^{3-} concentration in solution was measured using the ascorbic acid method [29] using UV spectrophotometer (Shimadzu UV-1800, Japan) at a wavelength of 880 nm. The PO_4^{3-} removal rate and equilibrium PO_4^{3-} adsorbed per gram of adsorbent was calculated using Equations 1 and 2:

$$\% \text{ Removal} = \frac{C_o - C_e}{C_o} \times 100 \quad (1)$$

$$Q_e = \frac{C_0 - C_e}{M} \times V \quad (2)$$

Where C_o and C_e represent the initial and residual PO_4^{3-} ion concentrations ($mg \cdot L^{-1}$) in the liquid phase, Q_e ($mg \cdot g^{-1}$) denotes the amount of PO_4^{3-} adsorbed per unit weight (g) of the adsorbent, M represents the mass of the adsorbent (g), and V is the volume of the PO_4^{3-} solution (L).

2.3 Phosphate desorption experiments and particle reusability

To determine the reusability of the tested adsorbents and the availability of adsorbed PO_4^{3-}, desorption experiment was carried out on PO_4^{3-}-loaded samples. The PO_4^{3-} desorption rate was studied using two solvent solutions, i.e. distilled water and various NaOH concentrations, at different time intervals (10-60 min). The particles were equally divided into two parts (approximately 0.25g for each part) and dispersed into two solvent solutions. For each desorption trial, 50 mL of either distilled water or NaOH were added to the PO_4^{3-} enriched material (0.25 g). The suspensions were shaken at 150 rpm (25 °C for 1 h) and filtered as previously described in the sorption trails. The residual PO_4^{3-} concentrations in the supernatants samples as previously using UV spectrophotometer. Seven adsorption and desorption cycles were conducted to investigate the potential reusability of regenerated particles with the adsorption performance measured in each cycle. Prior to re-adsorption trials, the particles were dried at 105 °C for 12 h and then reused for subsequent PO_4^{3-} adsorption and desorption processes. The PO_4^{3-} desorption rates (%) were calculated using the expression in Equation 3:

Desorption efficiency = $\frac{C*V}{X*m} \times 100\%$ (3)

Herein, C ($mg \cdot L^{-1}$) is the PO_4^{3-} concentration in desorption solution, q ($mg \cdot g^{-1}$) is the amount of PO_4^{3-} adsorbed prior to desorption, m (g) amount of adsorbent used in desorption experiments, V (L) is the volume of desorption solution.

2.3. Modeling

Three well-known models were used to gain a deeper insight into the adsorption kinetics (first- or second-order) [30], type (monolayer or multilayer) [31, 32] and thermodynamics (endothermic or exothermic). The three models used were: pseudo-first-order, pseudo-second-order, and intra-particle diffusion models, expressed as Eqs. 4–6

$\ln (Q_1 - Q_t) = \ln(Q_1) - \frac{\lambda_1}{2.0303} t$ (Pseudo first order) (4)

$\frac{t}{Q_t} = \frac{1}{\lambda_2 (Q2)^2} + \frac{1}{Q_2} t$ (Pseudo second order) (5)

$qt = K_d t^{1/2} + C$ (Intra particle model) (6)

where Q_1, and Q_2 ($mg \cdot g^{-1}$) indicate PO_4^{3-} adsorbed at the equilibrium state, Q_t is the PO_4^{3-} adsorbed at a given time (t), and λ_1 and λ_2 (min^{-1}) are the rate constants calculated from the linear plot of ln (Q_e-Q_t) against time (t) and t/Qt against t, for the pseudo-first and second order models, respectively

Langmuir (Equation 7) and Freundlich (Equation 8) models were employed to investigate the type of PO_4^{3-} adsorption.

$\frac{Ce}{Q_e} = \frac{1}{\alpha\beta} + \frac{\alpha}{C_e}$ (7)

$\ln Q_e = \ln K_f + \frac{1}{n} \ln C_e$ (8)

where C_e (mg L^{-1}) represents the equilibrium PO_4^{3-} concentration, α (mg·g^{-1}) indicates the maximum monolayer adsorption, β (L mg^{-1}) represents the adsorption equilibrium constant, K_f represents the amount of PO_4^{3-} ions adsorbed for unit equilibrium concentration, and n defines the intensity of the adsorption process. The Langmuir constants include α and β, while K_f and n are the Freundlich constants. In Langmuir model, both 'α' and 'β' were determined through the linear plot of (C_e/Q_e) versus C_e as the slope (1/α) and intercept (1/$\alpha\beta$), respectively. Similarly, the Freundlich model as plotted by ln Qe against ln Ce, the values of the constants *'Kf'* and 'n' were determined as the intercept (ln *Kf*) and slope (*1/n*).

The thermodynamic equilibrium constant, K_c, is defined as [33]

$$K_c = \frac{C_o - C_e}{C_e} \tag{9}$$

Where C_o and C_e (mg·L^{-1}) are the initial and equilibrium PO_4^{3-} solution concentrations, respectively. The Gibb's free energy change (ΔG°) of the process can be related to K_c by Equations 10 and 11.

$$\Delta G^o = -RTlnK_c \tag{10}$$

$$ln\, K_c = -\frac{\Delta G^o}{RT} = -\frac{\Delta H^o}{RT} + \frac{\Delta S^o}{R} \tag{11}$$

where T the is temperature in K, and R is the ideal gas constant of 8.314 J·mol^{-1}·K^{-1} [34]. Thus, from the linear plot of *lnKc* versus 1/T, the enthalpy (ΔH°) and entropy (ΔS°) values were calculated from the slope and intercept, respectively.

3. Results and Discussion

3.1 Characterization of synthesized iron oxides

The characterized physicochemical properties for the studied iron minerals; ferrihydrite (F) goethite (G), and magnetite (M) are reported in Table 1. Particle size distributions of the studied materials followed the order F < M < G, while a reverse sequence was observed for the BET surface area. The characteristics of large BET surface area and single point total pore volume strongly showed the suitability of these materials for PO_4^{3-} removal from aqueous solution. The points of zero charge values were 8.1 for F, 7.5 for M, and 8.4 for G, respectively. FTIR and IRD characterization of these minerals before and after adsorption is presented in Fig. 1. Additional peaks corresponding to P=O vibration in FTIR characterization were identified at 1081 cm^{-1} for F, 1125 cm^{-1} for M, and 1098 cm^{-1} for G after adsorption. This was also consistent with the elemental analyses and EDS spectra of studied materials (Fig. 2). Diffraction peaks at 2θ in XRD analysis could be assigned to nanoparticles.

In addition, the morphologies of these three studied iron minerals were identified using TEM images (Fig. S1 a, c, e in supplementary material). F was characterized by smaller particle with non-uniform sizes and shapes due to its porous nature, and M on the other hand was characterized by a cubic packed shape with measurable sized particles. The shape of G was spherical in nature. The SEM images (Fig. S1 b, d, f in supplementary material) showed more porous aggregate structures for F and more crystalline structure for M and G.

3.2 Adsorption performance

3.2.1 Effect of adsorbent dosage

The effect of adsorbent dosage on phosphorus adsorption was studied by varying the adsorbent dosage from 1 to 15 $g \cdot L^{-1}$ with an initial PO_4^{3-} concentration of 100 mg L^{-1} at pH 7.0 ± 0.1 and 25 °C. Results in Fig. S2a in supplementary material clearly show a general trend of increased PO_4^{3-} removal with an increase in adsorbent dosage. The adsorbed P increased from 15%, 17%, and 21% at 1 $g \cdot L^{-1}$ adsorbent dosage to the

maximum removal of 77%, 81% and 89% at 5 $g \cdot L^{-1}$ adsorbent dosage for G, M and F respectively. It was attributed to the higher number of binding sites for the studied three minerals [38]. Furthermore, adsorbent particle aggregation and repulsive forces between binding sites may also cause incremental improvement in PO_4^{3-} removal [39]. However, PO_4^{3-} removal kept maintained at adsorbent dosages above 5 $g \cdot L^{-1}$, possibly due to resistance in the PO_4^{3-} mass transfer from the bulk liquid to solid surface sites at high adsorbent dosage.

3.2.2 Effect of reaction time

The reaction time plays a vital role in the sorption process. It defines the equilibrium point between PO_4^{3-} ions and sorbents, as well as describing PO_4^{3-} adsorption kinetics. To investigate the effect of time on PO_4^{3-} sorption, the varied reaction time was tested from 5 to 480 min using an initial PO_4^{3-} concentration of 100 $mg \cdot L^{-1}$ at pH 7 ± 0.1 and 35 °C (Fig. S1b in supplementary material). The P adsorption rate generally increased with time. However, after a fast adsorption period occurred for 0–120 min, the adsorption of the tested minerals slowed down and then become saturated. The adsorption capacity was tested to be 9 $mg \cdot g^{-1}$ during the fast adsorption phase. Equilibrium was achieved to be 8.96 $mg \cdot g^{-1}$ for F, 7.95 $mg \cdot g^{-1}$ for M, and 7.16 $mg \cdot g^{-1}$ for G at 120 min. Therefore, further experiments were run at the time scheme of 120 min.

3.2.3 Effect of initial concentration

As the initial concentration of PO_4^{3-} ions varied from 200 to 1000 $mg \cdot L^{-1}$, the adsorbed P increased from 15 to 50 $mg \cdot g^{-1}$ for F, 14 to 44 $mg \cdot g^{-1}$ for M, and 13 to 40 $mg \cdot g^{-1}$ for G, respectively (Fig. S1c in supplementary material). The maximum adsorption capacities of 50 $mg \cdot g^{-1}$, 44 $mg \cdot g^{-1}$, and 40 $mg \cdot g^{-1}$ for F, M, and G, respectively, were observed at initial PO_4^{3-} concentrations of 1000 $mg \cdot L^{-1}$, while minimum values were obtained for initial PO_4^{3-} concentrations of 200 $mg \cdot L^{-1}$. The increase in adsorption capacity with increased initial PO_4^{3-} ion concentration has been well reported and can be explained using Equation 2. The adsorbent surface contains a fixed number of binding sites, many of which remain unoccupied at low initial PO_4^{3-} concentrations. However, at higher initial concentrations, they can be quickly unoccupied. Furthermore, higher surface area

(Table 2) created a measurable difference in the adsorption capacity of the studied three minerals at initial concentration of 1000 mg·L^{-1}.

3.2.4 Effect of pH

As pH increased from 6 to 9, the adsorption capacity decreased from 9.57 to 5.97 mg·g^{-1} for F, from 8.77 to 4.96 mg g^{-1} for M, and from 7.63 to 4.24 mg g^{-1} for G, respectively (Fig. S1d). This was because the variation in operating pH also changes the iron mineral properties (surface charge) and adsorbate degree of ionization and dissociation of functional groups [40, 41]. The pH related PO_4^{3-} dissociation equilibria in the liquid phase can be expressed as:

$$H_3PO_4^- \rightarrow H_2PO_4 \rightarrow HPO_4^{2-} \rightarrow PO_4^{3-} \quad (12)$$

If taking the dissociation constant (pK_a) into account, i.e., pKa_1 =2.15 for H_3PO_4, pKa_2 = 7.20 for HPO_4^{2-} and pKa_3 = 12.33 for PO_4^{3-}, it's noteworthy that solution pH determines the relevant PO_4^{3-} species dominance and can influence the strength of electrostatic attraction. Moreover, the surface charges on the minerals at a pH_{pzc} of 8.1 for F, 7.5 for M, and 8.4 for G may also explain the enhanced PO_4^{3-} sorption where the positive charge builds up below the pH_{pzc}, while negative charge accumulates above the pH_{pzc}. Strong competition thus occurs between PO_4^{3-} species ($H_2PO_4^-$, HPO_4^{2-}, and PO_4^{3-}) and hydroxyl (OH^-) ions at higher pH, creating strong repulsions between phosphate and hydroxyl ions that reduces adsorption. However, PO_4^{3-} adsorption can also be stimulated and enhanced by the presence of free hydroxyl ions (OH^-), which could be replaced by PO_4^{3-} ions on the iron oxyhydroxide surface [42]. On the other hand, PO_4^{3-} may also be enhanced by the formation of inner-sphere complexes, such as monodentate, bidentate, mononuclear, and binuclear complexes [43, 44]. Similar findings have been given for the adsorption of anionic species onto M [38], hematite [45], and F [19]. In principal, our results show that the difference between the increased sorption capacity of adsorbents at pH 6 and pH 7 is < 1 mg g^{-1}. Thus, the decrease in PO_4^{3-} adsorption with an increase in pH might be mainly due to electrostatic attraction. However, the larger decrease in PO_4^{3-} adsorption to magnetic particles above the pH_{pzc} was not only due to reduction in electrostatic interaction, but also reduced inner-sphere complexation between the PO_4^{3-} and surface groups [19]. In the case of pH, PO_4^{3-} sorption to F does not depend solely upon the larger surface area, but also upon its point of zero charge.

3.2.5 Ionic strength effect

The results of the influence of ionic strength on PO_4^{3-} removal are displayed in Fig. S2e in supplementary material. It is observed that an increase in ionic strength from 0.001 to 0.01 caused a 10% increase in PO_4^{3-} removal. However, no significant change in PO_4^{3-} removal was observed afterward, with variations in ionic strength from 0.01 to 0.05 N NaCl. Generally, the ionic strength effect is linked to the adsorbent particle surface reactions, as it describes the formation of inner or outer-sphere complexes during targeted species elimination [46]. As such, the electrostatically adsorbed PO_4^{3-} ions that form outer-sphere complexes compete with background electrolytes for adsorbent surface sites [47]. Thus, a decreased PO_4^{3-} adsorption with increased electrolyte concentrations is expected as a consequence of outer-sphere complexation [19]. Conversely, in our experiments, the increased PO_4^{3-} adsorption values for all adsorbents with increasing ionic strength corroborate the findings of previous studies that used F [19], M [47] and G [48]. This evidence further attributes ion effect to the involvement of inner-sphere mechanisms that are directly analogous to the surface groups via ligand exchange. In slightly lower ion gradient, PO_4^{3-} adsorption occurred by replacing weakly adsorbed electrolyte ions that form outer-sphere complexes [49]. Hence, the observed lack of significant change in the adsorption capacity with increasing ionic strength implies that the inner-sphere mechanisms become the marginal sorption rate limiting factors.

3.2.6 Sorption isotherm

The equilibrium studies of adsorption explain the interaction between the adsorbent and PO_4^{3-} ions. So this information normally assists to optimize, design and operate the adsorption process [50]. As the Langmuir (Eq. 7) and Freundlich (Eq. 8) isotherm models are generally applied, they are also used to adsorption data in this study (Fig. 3d). The correlation coefficient value ($R^2 > 0.95$) indicates that the Langmuir model adequately fits to describe the equilibrium adsorption of PO_4^{3-} ions onto iron particles. The Langmuir model can also be used to determine the feasibility of PO_4^{3-} ion adsorption onto iron particles based on the R_L which is dimensionless constant expressed as =

$1/(1+\beta C_e)$. Adsorption is considered favorable if $0 < R_L < 1$, whereas $R_L > 1$ indicates unfavorable adsorption, $R_L = 1$ indicates linear adsorption, and $R_L = 0$ indicates irreversible adsorption. The R_L values for the three adsorbents in this study ranged from 0.621 to 0.653, implying favorable adsorption for PO_4^{3-} ions from aqueous solution.

The profile of the Freundlich model are also provided in Fig. 3e. This model fits even better ($R^2 > 0.992$) to the adsorption data as compared to the Langmuir model. The application of the Freundlich model suggests that the surfaces of the iron minerals are heterogeneous and sorption of PO_4^{3-} ions on particles occurs in the form of multilayers. The higher K_F values imply an easy uptake of PO_4^{3-} ions from aqueous solution with the high adsorptive capacity of iron bearing adsorbents. Values of $1/n > 1$ confirmed chemisorption as the main adsorption mechanism in this study for all adsorbents. The highest R^2 value of F as exhibiting higher sorption capacity indicates relationship between the porous nature of F and multi-layer sorption of PO_4^{3-} ions. The maximum adsorption capacity values of 66.6, 57.8, and 50.5 $mg \cdot g^{-1}$ for F, M, and G, respectively obtained in this study can be compared with the literature (Table 3). Therefore, the tested minerals in this study show practical capabilities to remove PO_4^{3-} from real wastewater.

3.2.7 Adsorption Kinetics

Kinetics for the adsorption of PO_4^{3-} ions onto the three studied particles minerals were evaluated using three models: the pseudo–first-order (Eq. 4), pseudo-second-order (Eq. 5), and intra-particle diffusion (Eq. 6). The performance of applying these models are presented in Fig. 3 and the detailed parametric data are provided in Table 4. Results show that the pseudo-first-order ($R^2 \leq 0.70$) model does not fit as well as the pseudo-second-order ($R^2 \geq 0.993$) and intra-particle diffusion ($R^2 \geq 0.936$) models for all three studied minerals. The calculated q_e values from pseudo-second-order model were closer to the experimental values (q_{exp}). The fitness of the pseudo-second-order model can also be verified by calculating the percentage deviation between the experimental amount of adsorbed PO_4^{3-} (qe_{exp}) and the calculated amount (qe_{cal}) [50]:

$$\%q_{deviation} = \left(qe_{exp} - qe_{cal} * 100\right)/qe_{cal}\right) \quad (13)$$

The adequacy of the pseudo–second-order model implies that adsorption occurs mainly via chemisorption. This conclusion was also established by the fitting of the Freundlich isotherm. Similar kinetic trends have also been reported in the literature [30, 39].

Although the results from Pseudo-second-order model suggested the mechanism of chemical sorption of P onto the tested three minerals, it might be still apparent that the adsorption of PO_4^{3-} may occur simultaneously via different pathways, e.g. film or pore diffusion. To evaluate the role played by pore diffusion, the intra-particle-diffusion model was applied to the kinetic data (Fig. 3c and Table 3). The bilinear trend reveals two or more involved mechanisms. The linear trend from the intra-particle-diffusion model indicates film diffusion. However, the straight lines did not pass through the origin ($C \neq 0$), implying the co-existence of both film and intra-particle diffusion mechanisms. The intra-particle diffusion phase appears to be slower than the film diffusion due to the narrow pores and possible electrostatic repulsion between adsorbed and unabsorbed PO_4^{3-} ions. Similar trends have also been reported for PO_4^{3-} adsorption onto iron-based adsorbents [13].

3.2.8 Adsorption Thermodynamics

The thermodynamic parameters for PO_4^{3-} adsorption at different temperatures are shown in Table 5. The relationship between temperature and PO_4^{3-} adsorption was presented in Fig. 3f. The maximum PO_4^{3-} adsorption were found to be 8.52 mg g^{-1} for F, 7.32 mg g^{-1} for M, and 7.16 mg·g^{-1} for G. Increased temperature caused an increase in the adsorption capacity and favoured the diffusion of unabsorbed PO_4^{3-} ions onto the iron mineral surfaces [51]. The overall negative Gibbs energy ($\Delta G°$) values in Table 5 indicate the spontaneous PO_4^{3-} sorption [39]. The increased Kc values as a function of increased temperature and positive enthalpy change ($\Delta H°$) indicate an endothermic process for the adsorption of PO_4^{3-} ions onto the studied minerals [42, 44]. Several researchers have also reported this endothermic and random process [52, 53]. The positive values of entropy change ($\Delta S°$) suggest greater randomness between the iron and PO_4^{3-} solution interface [54].

3.3 Desorption performance

With an objective of particles reusability and recycling of PO_4^{3-} as a source of fertilizer, an understanding about PO_4^{3-} desorption after being particles saturation is an important aspect. In this study, the PO_4^{3-} desorbability was explained in terms of total desorbed PO_4^{3-} to the total amount of adsorbed PO_4^{3-} from particles using water and in the present of different strength alkaline solvents. The reason of using alkaline solvent for PO_4^{3-} recovery is that, in our study, overall PO_4^{3-} adsorption was decreased with increasing solution pH, which was an evidence that adsorbed PO_4^{3-}, could be easily detached from particles in a solution with higher pH.

The results in Fig. 4 showed the dynamics of PO_4^{3-} desorption performance depending on time and solvent concentration. Within 60 min, the amount of released PO_4^{3-} was increased as increase of desorption time. With increasing desorption time to a maximum of 60 min, the amount of released PO_4^{3-} also increased. Likewise, increased concentration of desorption solvent from 0.1-1 N, also resulted in an increase of released PO_4^{3-} . Optimum desorption rates of 75, 85 and 82 %, were achieved at 1 N solvent concentration for F, M and G, respectively. This phenomenon could be well explained in term of adsorption competition between OH^- and PO_4^{3-} anion on the surface of tested minerals [41, 47]. In addition, temperature also plays a vital role in PO_4^{3-} desorption from the synthesized iron oxides. Temperature at 35°C in this study was found to be optimum for desorption efficiency of 88.3, 95.1 and 92.2% for F, M and G, respectively. The good desorption capacity of PO_4^{3-} from the tested three minerals in this study provides a potentially scalable way of adsorbent regeneration.

In general, the adsorption capacity ($mg \cdot g^{-1}$) as well as the percentage adsorption removal (%) of P by regenerated particles might be lower than that of freshly prepared materials due to the loss of active binding sites. This was also observed in the current study. As the results shown in Fig.5, the desorption capacity of the tested minerals at 1st regeneration cycle was 4.39 $mg \cdot g^{-1}$for M, 3.51 $mg \cdot g^{-1}$ for G and 3.13 $mg \cdot g^{-1}$ for F, respectively. However, it was decreased by 34%, 32% and 28% for M, G and F at the 7th regeneration cycle, respectively.

4. Conclusion

Three iron oxides were evaluated for adsorption and desorption of PO_4^{3-} from aqueous solution. Higher adsorption was found with longer contact time and higher temperature. Maximum monolayer adsorption capacities of 66.6 $mg \cdot g^{-1}$ for ferrihydrite, 57.8 $mg \cdot g^{-1}$ for magnetite, and 50.5 $mg \cdot g^{-1}$ for goethite were exhibited. Moreover, the PO_4^{3-} adsorption process was found to be endothermic and spontaneous. Electrostatic attraction and surface precipitation interactions between adsorbate and adsorbent were the key mechanistic pathways for PO_4^{3-} removal from wastewater rather than intraparticle diffusion. The tested minerals can be easily regenerated due to the high desorption performance of adsorbed PO_4^{3-} in alkaline solutions.

Conflict of interest

The authors declare no conflict of interest whether financial or relational during the preparation and submission of this work.

Acknowledgement

This work was financed by grants from the project of “Research Fund for International Young Scientist (51650110489)”.

References

[1] P.S. Lau, N.F.Y. Tam, Y.S. Wong, Wastewater nutrients (N and P) removal by carrageenan and alginate immobilized Chlorella vulgaris, Environ. Technol.18(9) (1997) 945-951.

[2] J. Van der Houwen, E. Valsami-Jones, The application of calcium phosphate precipitation chemistry to phosphorus recovery: the influence of organic ligands, Environ. Technol. 22 (2001) 1325-1335.

[3] Y.Z. Peng, X.L. Wang, B.K. Li, Anoxic biological phosphorus uptake and the effect of excessive aeration on biological phosphorus removal in the A(2)O process, Desalination 189(1-3) (2006) 155-164.

[4] A. Muhmood, S. Wu, J. Lu, Z. Ajmal, H. Luo, R. Dong, Nutrient recovery from anaerobically digested chicken slurry via struvite: Performance optimization and interactions with heavy metals and pathogens, Sci. Total Environ. 635 (2018) 1-9.

[5] E.N. Peleka, P.P. Mavros, D. Zamboulis, K.A. Matis, Removal of phosphates from water by a hybrid flotation–membrane filtration cell, Desalination 198 (2006) 198-207.

[6] M.T. Ghaneian, G. Ghanizadeh, M.T.H. Alizadeh, M.H. Ehrampoush, F.M. Said, Equilibrium and kinetics of phosphorous adsorption onto bone charcoal from aqueous solution, Environ Technol. 35 (2014) 882-890.

[7] M. Usman, J.M. Byrne, A. Chaudhary, S. Orsetti, K. Hanna, C. Ruby, A. Kappler, S.B. Haderlein, Magnetite and Green Rust: Synthesis, Properties, and Environmental Applications of Mixed-Valent Iron Minerals, Chem. Rev. 118(7) (2018) 3251-3304.

[8] M. Zhang, K. Zheng, J. Jin, X. Yu, L. Qiu, S. Ding, H. Lu, J. Cai, P. Zheng, Effects of Fe (II)/P ratio and pH on phosphorus removal by ferrous salt and approach to mechanisms, Sep. Purf. Technol. 118 (2013) 801-805.

[9] W. Zeng, L. Li, Y.y. Yang, X.d. Wang, Y.z. Peng, Denitrifying phosphorus removal and impact of nitrite accumulation on phosphorus removal in a continuous anaerobic–anoxic–aerobic ((A2O) process treating domestic wastewater, Enzyme Microb. Technol. 48 (2011) 134-142.

[10] K.H. Yeon, H. Park, S.H. Lee, Y.M. Park, S.H. Lee, M. Iwamoto, Zirconium mesostructures immobilized in calcium alginate for phosphate removal, Korean J. Chem. Eng. 25 (2008) 1040-1046.

[11] J.H. Park, D.I. Jung, Removal of total phosphorus (TP) from municipal wastewater using loess, Desalination. 269 (2011) 104-110.

[12] A. Ahmad, M. Rafatullah, O. Sulaiman, M.H. Ibrahim, Y.Y. Chii, B.M. Siddique, Removal of Cu (II) and Pb (II) ions from aqueous solutions by adsorption on sawdust of Meranti wood, Desalination. 247 (2009) 636-646.

[13] J. Lalley, C. Han, X. Li, D.D. Dionysiou, M.N. Nadagouda, Phosphate adsorption using modified iron oxide-based sorbents in lake water: kinetics, equilibrium, and column tests, Chem. Eng. J. 284 (2016) 1386-1396.

[14] E.W. Shin, J.S. Han, M. Jang, S.H. Min, J.K. Park, R.M. Rowell, Phosphate adsorption on aluminum-impregnated mesoporous silicates: surface structure and behavior of adsorbents, Environ. Sci. Technol. 38 (2004) 912-917.

[15] M.S. Onyango, D. Kuchar, M. Kubota, H. Matsuda, Adsorptive removal of phosphate ions from aqueous solution using synthetic zeolite, Ind. Eng. Chem. Res. 46 (2007) 894-900.

[16] S. Kizito, H. Luo, S. Wu, Z. Ajmal, T. Lv, R. Dong, Phosphate recovery from liquid fraction of anaerobic digestate using four slow pyrolyzed biochars: Dynamics of adsorption, desorption and regeneration, J. Environ. Manage. 201 (2017) 260-267.

[17] E. Lopez, B. Soto, M. Arias, A. Nunez, D. Rubinos, M. Barral, Adsorbent properties of red mud and its use for wastewater treatment, Water Res. 32 (1998) 1314-1322.

[18] D. Georgantas, H. Grigoropoulou, Orthophosphate and metaphosphate ion removal from aqueous solution using alum and aluminum hydroxide, J. Colloid Interf. Sci. 315 (2007) 70-79.

[19] M. Mallet, K. Barthelemy, C. Ruby, A. Renard, S. Naille, Investigation of phosphate adsorption onto ferrihydrite by X-ray photoelectron spectroscopy, J. Colloid Interf. Sci. 407 (2013) 95-101.

[20] T. Daou, S. Begin-Colin, J. Greneche, F. Thomas, A. Derory, P. Bernhardt, P. Legare, G. Pourroy, Phosphate adsorption properties of magnetite-based nanoparticles, Chem. Mater. 19 (2007) 4494-4505.

[21] R. Chitrakar, S. Tezuka, A. Sonoda, K. Sakane, K. Ooi, T. Hirotsu, Phosphate adsorption on synthetic goethite and akaganeite, J. Colloid Interf. Sci. 298 (2006) 602-608.

[22] K. Barthelemy, S. Naille, C. Despas, C. Ruby, M. Mallet, Carbonated ferric green rust as a new material for efficient phosphate removal, J. Colloid Interf. Sci. 384 (2012) 121-127.

[23] N. Karapinar, E. Hoffmann, H.H. Hahn, Magnetite seeded precipitation of phosphate, Water Res. 38 (2004) 3059-3066.

[24] L. Zeng, X. Li, J. Liu, Adsorptive removal of phosphate from aqueous solutions using iron oxide tailings, Water Res. 38(5) (2004) 1318-1326.

[25] U. Schwertmann, R. Cornell, Methods of characterization, Iron Oxides in the Laboratory: Preparation and Characterization (2000) 27-54.

[26] M. Usman, M. Abdelmoula, K. Hanna, B. Gregoire, P. Faure, C. Ruby, Fe II induced mineralogical transformations of ferric oxyhydroxides into magnetite of variable stoichiometry and morphology, J. Solid State Chem. 194 (2012) 328-335.

[27] A. Jaiswal, S. Banerjee, R. Mani, M. Chattopadhyaya, Synthesis, characterization and application of goethite mineral as an adsorbent, J. Environ. Chem. Eng. 1(3) (2013) 281-289.

[28] S. Rajput, C.U. Pittman, D. Mohan, Magnetic magnetite (Fe 3 O 4) nanoparticle synthesis and applications for lead (Pb 2+) and chromium (Cr 6+) removal from water, J. Colloid Interf. Sci. 468 (2016) 334-346.

[29] APHA (American Public Health Association), Standard methods for the examination of water and wastewaterWastewater, Washington, DC, USA APHA., (1995).

[30] Y.S. Ho, G. McKay, Pseudo-second order model for sorption processes, Process Biochem. 34 (1999) 451-465.

[31] l. Langmuir, The adsorption of gases on plane surfaces of glass, mica, and platinum, J. Am. Chem. Soc. 40 (1918) 1361-1368.

[32] H. Freundlich, Over the adsorption in solution, J. Phys. Chem. Soc. 57(385) (1906) e470.

[33] P.V. Nidheesh, R. Gandhimathi, S.T. Ramesh, T.S.A. Singh, Kinetic analysis of crystal violet adsorption on to bottom ash, Turk. J. Eng. Environ. Sci. 36 (2012) 249-262.

[34] Z. Aksu, Determination of the equilibrium, kinetic and thermodynamic parameters of the batch biosorption of nickel (II) ions onto Chlorella vulgaris, Process Biochem. 38 (2002) 89-99.

[35] M.I. Tejedor-Tejedor, M.A. Anderson, Protonation of phosphate on the surface of goethite as studied by CIR-FTIR and electrophoretic mobility, Langmuir;(United States) 6 (1990).

[36] J. Lu, H. Liu, R. Liu, X. Zhao, L. Sun, J. Qu, Adsorptive removal of phosphate by a nanostructured Fe–Al–Mn trimetal oxide adsorbent, Powder Technol. 233 (2013) 146-154.

[37] M. Dai, L. Xia, S. Song, C. Peng, A. Lopez-Valdivieso, Adsorption of As(V) inside the pores of porous hematite in water, J. Hazard. Mater. 307 (2016) 312-317.

[38] S.Y. Yoon, C.G. Lee, J.A. Park, J.H. Kim, S.B. Kim, S.H. Lee, J.W. Choi, Kinetic, equilibrium and thermodynamic studies for phosphate adsorption to magnetic iron oxide nanoparticles, Chem. Eng. J. 236 (2014) 341-347.

[39] N.Y. Mezenner, A. Bensmaili, Kinetics and thermodynamic study of phosphate adsorption on iron hydroxide-eggshell waste, Chem. Eng. J. 147 (2009) 87-96.

[40] B. Nandi, A. Goswami, M. Purkait, Adsorption characteristics of brilliant green dye on kaolin, J. Hazard. Mater. 161 (2009) 387-395.

[41] J. Choi, J. Chung, W. Lee, J.-O. Kim, Phosphorous adsorption on synthesized magnetite in wastewater, J. Ind. Eng. Chem. 34 (2016) 198-203.

[42] Z. Ren, L. Shao, G. Zhang, Adsorption of phosphate from aqueous solution using an iron–zirconium binary oxide sorbent, Water, Air, Soil Pollut. 223 (2012) 4221-4231.

[43] H. Zeng, B. Fisher, D.E. Giammar, Individual and competitive adsorption of arsenate and phosphate to a high-surface-area iron oxide-based sorbent, Environ. Sci. Technol. 42 (2007) 147-152.

[44] B. Pan, J. Wu, B. Pan, L. Lv, W. Zhang, L. Xiao, X. Wang, X. Tao, S. Zheng, Development of polymer-based nanosized hydrated ferric oxides (HFOs) for enhanced phosphate removal from waste effluents, Water Res. 43 (2009) 4421-4429.

[45] G. Horanyi, P. Joo, Some peculiarities in the specific adsorption of phosphate ions on hematite and γ-Al2O3 as reflected by radiotracer studies, J. Colloid Interf. Sci. 247 (2002) 12-17.

[46] J. Antelo, S. Fiol, C. Perez, S. Marino, F. Arce, D. Gondar, R. Lopez, Analysis of phosphate adsorption onto ferrihydrite using the CD-MUSIC model, J. Colloid Interf. Sci. 347 (2010) 112-119.

[47] Y.J. Tu, C.F. You, C.K. Chang, M.H. Chen, Application of magnetic nano-particles for phosphorus removal/recovery in aqueous solution, J. Taiwan Inst. Chem. Eng. 46 (2015) 148-154.

[48] J. Antelo, M. Avena, S. Fiol, R. Lopez, F. Arce, Effects of pH and ionic strength on the adsorption of phosphate and arsenate at the goethite–water interface, J. Colloid Interf. Sci. 285 (2005) 476-486.

[49] G. Zhang, H. Liu, R. Liu, J. Qu, Removal of phosphate from water by a Fe–Mn binary oxide adsorbent, J. Colloid Interf. Sci. 335 (2009) 168-174.

[50] M.S.U. Rehman, M. Munir, M. Ashfaq, N. Rashid, M.F. Nazar, M. Danish, J.I. Han, Adsorption of Brilliant Green dye from aqueous solution onto red clay, Chem. Eng. J. 228 (2013) 54-62.

[51] M. Alkan, M. Dogan, Y. Turhan, O. Demirbas, P. Turan, Adsorption kinetics and mechanism of maxilon blue 5G dye on sepiolite from aqueous solutions, Chem. Eng. J. 139 (2008) 213-223.

[52] Z.-l. Shi, F.-m. Liu, S.-h. Yao, Adsorptive removal of phosphate from aqueous solutions using activated carbon loaded with Fe(III) oxide, New. Carbon Mater. 26(4) (2011) 299-306.

[53] P.A. Trazzi, J.J. Leahy, M.H.B. Hayes, W. Kwapinski, Adsorption and desorption of phosphate on biochars, J. Environ. Chem. Eng 4(1) (2016) 37-46.

[54] L.g. Yan, Y.y. Xu, H.q. Yu, X.d. Xin, Q. Wei, B. Du, Adsorption of phosphate from aqueous solution by hydroxy-aluminum, hydroxy-iron and hydroxy-iron–aluminum pillared bentonites, J. Hazard. Mater 179 (2010) 244-250.

[55] C.S. Chiou, Y.F. Lin, H.W. Chen, C.C. Chang, S.H. Chang, Adsorption of Phosphate in Aqueous Solution by Magnetite Modified with Diethylenetriamine, J. Nanosci. Nanotechnol. J. 15 (2015) 2850-2857.

[56] N. Boujelben, J. Bouzid, Z. Elouear, M. Feki, F. Jamoussi, A. Montiel, Phosphorus removal from aqueous solution using iron coated natural and engineered sorbents, J. Hazard. Mater. 151 (2008) 103-110.

[57] J. Xiong, Z. He, Q. Mahmood, D. Liu, X. Yang, E. Islam, Phosphate removal from solution using steel slag through magnetic separation, J. Hazard. Mater. 152 (2008) 211-215.

[58] W. Xiong, J. Peng, Development and characterization of ferrihydrite-modified diatomite as a phosphorus adsorbent, Water Res. 42 (2008) 4869-4877.

[59] A.F. de Sousa, T.P. Braga, E.C.C. Gomes, A. Valentini, E. Longhinotti, Adsorption of phosphate using mesoporous spheres containing iron and aluminum oxide, Chem. Eng. J. 210 (2012) 143-149.

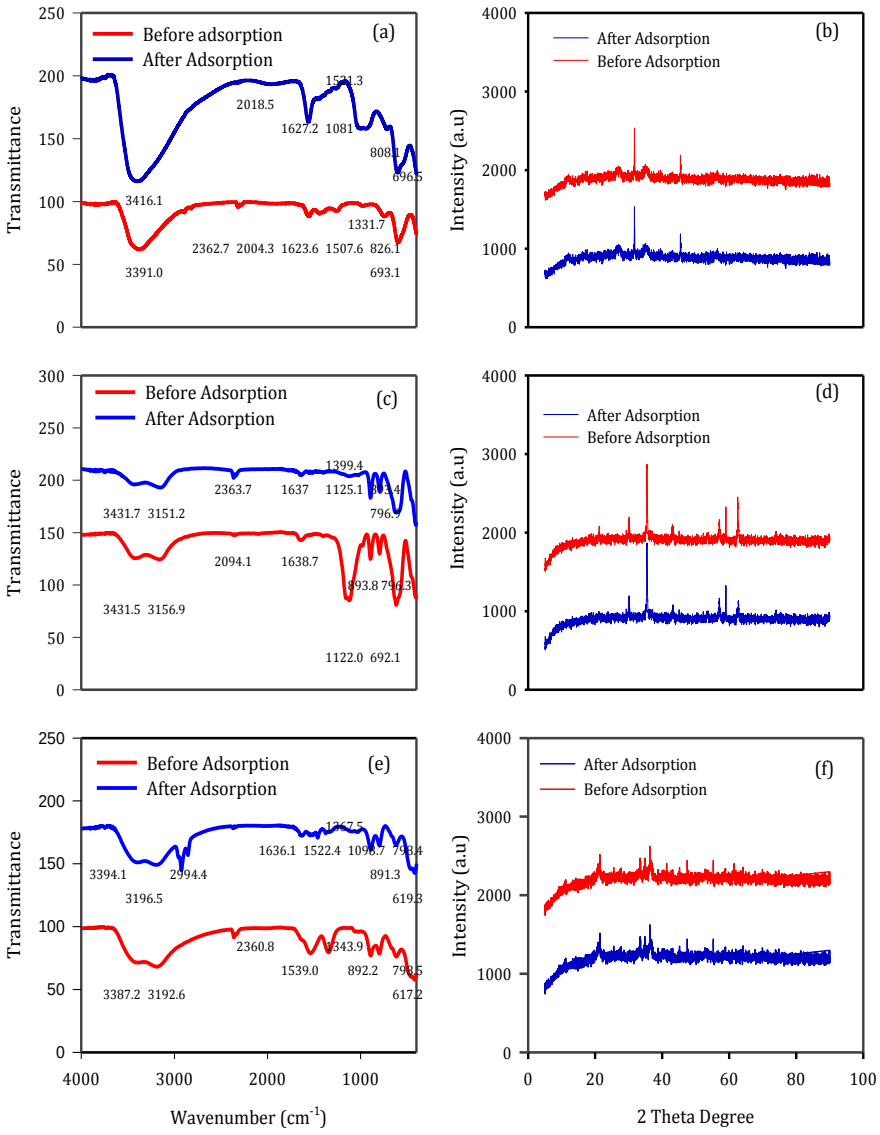

Fig.1. Comparison of XRD (Right) and FTIR (Left) spectra of ferrihydrite (a, b), magnetite (c, d), goethite (e, f) before and after adsorption.

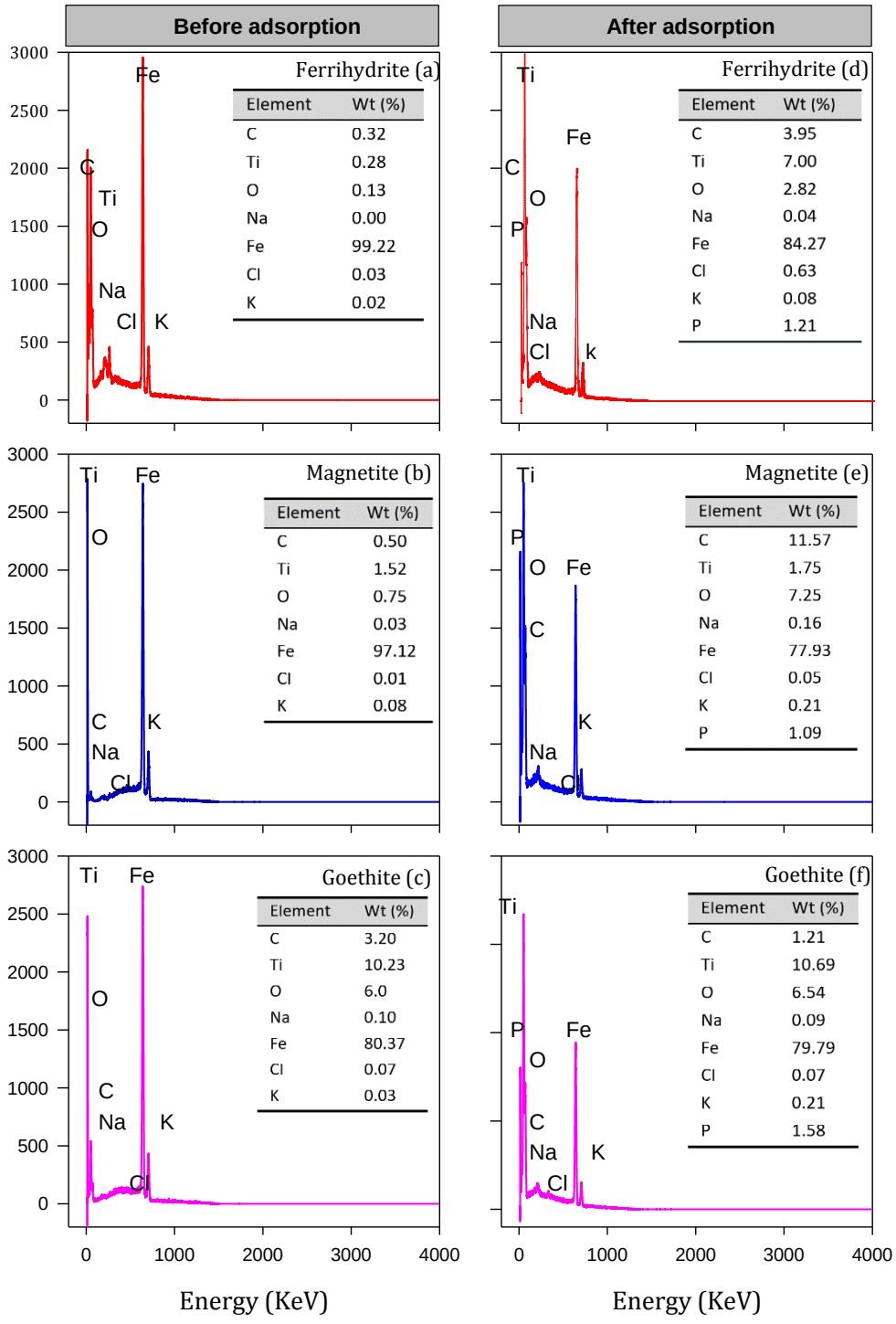

Fig.2. EDS spectra of various kind of iron minerals before PO_4^{3-} adsorption **(**a) Ferrihydrite (c) Magnetite (e) Goethite and after PO_4^{3-} adsorption (b) Ferrihydrite (d) Magnetite (f) Goethite

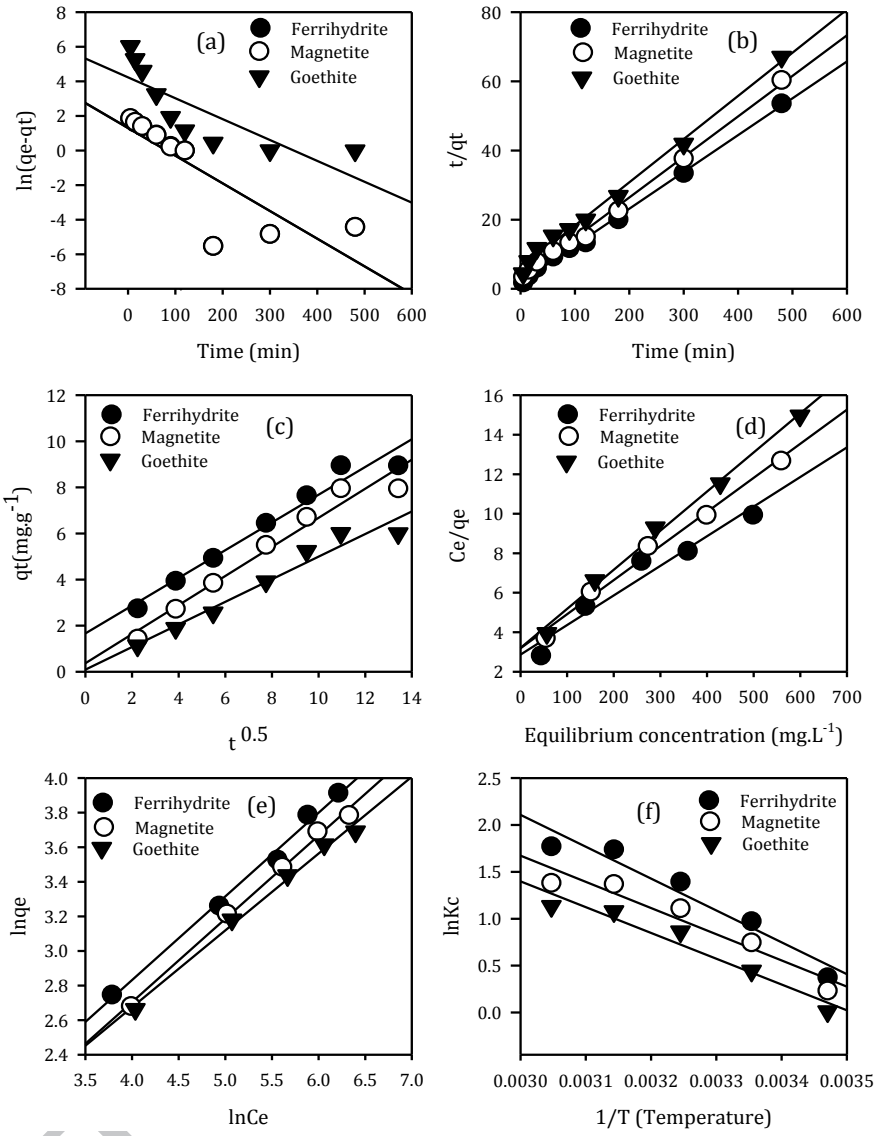

Fig.3. Modeling of PO_4^{3-} adsorption data via kinetic, equilibrium and thermodynamic simulations **(a)** Pseudo 1st order **(b)** Pseudo 2nd order **(c)** Intraparticle **(d)** Langmuir **(e)** Freundlich **(f)** Van't Hoff's model

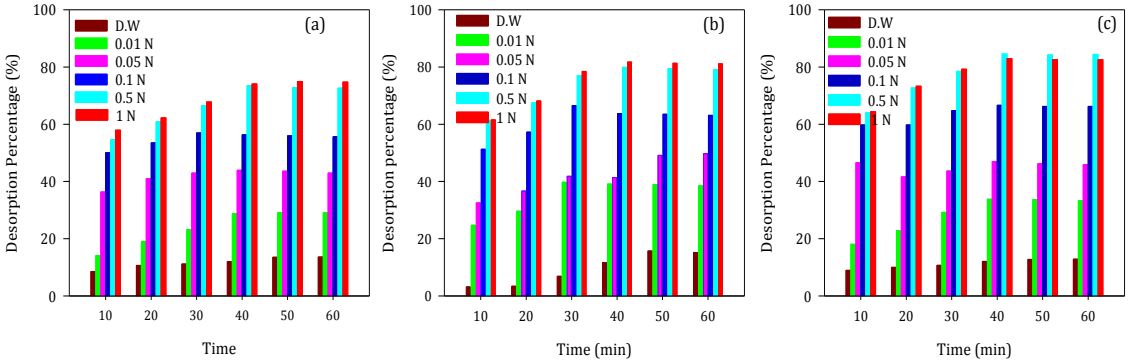

Fig.4. Phosphate desorption from various iron minerals using distil water and alkaline solution (**a)** Ferrihydrite **(b)** Magnetite **(c)** Goethite

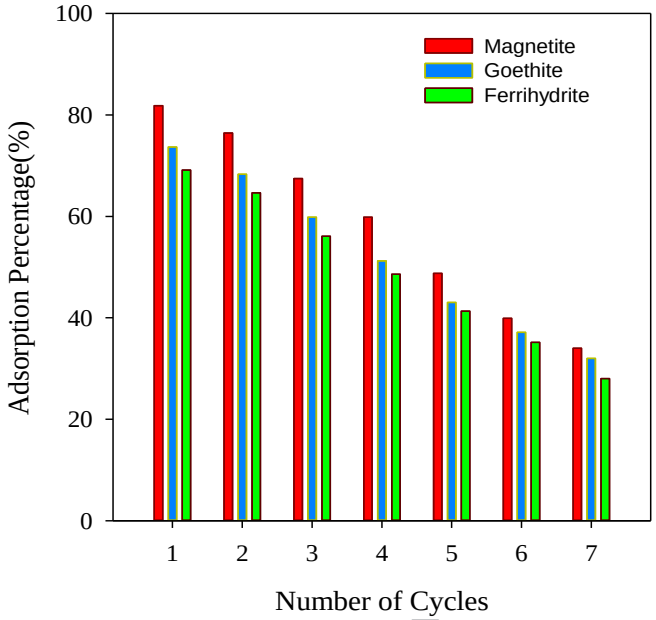

Fig.5. Different cycle number regarding particle reusability for phosphate recovery using various alkaline media concentration and distil water.

Table 1. Physico-chemical properties of experimental materials used in this study.

Note: SSA means Specific Surface Area, PZC means Point of Zero Charge.

Parameters	Unit	Ferrihydrite	Magnetite	Goethite
SSA	($m^2 \cdot g^{-1}$)	178.8	123.1	86.95
Particle Size	(nm)	4-30	32-55	83-120
PZC		8.1±1	7.5±1	8.4±1
Pore Volume	(ml/g)	0.327	0.416	0.112
Iron Content (Fe)	(%)	22.90	31.10	19.70

Table 2. Equilibrium phosphate concentration and adsorbed amount by different iron minerals at different initial phosphate concentration.

Initial Concentration (Co, mg·P L^{-1})	Equilibrium Concentration (Ce, mg·L^{-1})			Adsorbed Amount (mg·g^{-1})		
	F	M	G	F	M	G
200	43.9	54.00	65.2	16	15	13
400	138.9	150.8	159.3	26	24	22
600	259.3	273.3	287.1	34	32	30
800	358.5	398.8	448.4	44	40	37
1000	498.6	559.2	599.4	50	44	40

Note: F (Ferrihydrite), M (Magnetite), G (Goethite).

Table 3**:** Equilibrium experimental data interpretation as values obtained by Langmuir and Freundlich models.

Material	Langmuir			Freundlich		
	α (mg.g-1)	β(L.mg^{1}*10^{-3})	R_L^2	K_F (mg.g^{-1})	1/n	R_F^2
Ferrihydrite	66.6	5.3	0.9947	2.06	1.12	0.9926
Magnetite	57.8	5.8	0.9896	2.07	1.29	0.9959
Goethite	50.5	6.1	0.9506	2.04	1.10	0.9925

Table 4. Kinetic parameters obtained for phosphate sorption of different iron minerals particles.

Models	Ferrihydrite	Magnetite	Goethite
Pseudo 1st order			
Q_1 (mg·g^{-1})	3.72	3.71	3.49
λ_1*10^{-3}	33.1	32.5	8.01
R^2	0.70	0.69	0.65
% qe	152.7	129.9	126.9
Pseudo 2nd order			
Q_2 (mg·g^{-1})	8.96	7.96	7.16
λ_2*10^{-3}	0.05	0.02	0.01
$V=\lambda_2(Q_2)^2$ mg·g^{-1}·min^{-1}	4.09	1.77	0.70
R^2	0.997	0.996	0.994
%qe	4.91	7.16	11.87
Intraparticle			
K_d (mg·g^{-1}·min^{-1})	0.60	0.63	0.49
C (mg·g^{-1})	1.66	0.37	0.09
R^2	0.95	0.94	0.94
Q_{exp}	9.40	8.96	7.56

Table 5. Thermodynamic parameters for phosphate sorption in pure solution onto various iron minerals particles.

Temperature (K)	K_c	$-\Delta G^o$ (J/mol)	ΔH^o(kj·mol^{-1})	ΔS^o (j·mol K^{-1})	R^2
Ferrihydrite					
288.15	1.46	898.8	28.27	102.32	0.9405
298.15	2.65	2412.3			
308.15	4.04	3575.3			
318.15	5.69	4600.5			
328.15	5.88	4834.0			
Magnetite					
288.15	1.26	557.5	23.24	83.62	0.9264
298.15	2.11	1853.4			
308.15	3.04	2846.9			
318.15	3.94	3623.8			
328.15	3.99	3772.4			
Goethite					
288.15	1.01	25.5	22.87	80.24	0.9421
298.15	1.56	1099.3			
308.15	2.37	2210.3			
318.15	2.94	2852.8			
328.15	3.11	3091.9			

Table 6. Comparative analysis of the present study with previous studies.

Materials	Surface area ($m^2 \cdot g^{-1}$)	pH	q ($mg \cdot g^{-1}$)	References
Naturally iron oxides coated sand	6.97	5.0	0.88	(56)
Steel slag	2.09	5.5	5.3	(57)
Fe-Zn binary oxide	309	5.6	36	(49)
Ferrihydrite modified diatomite	211.1	8.5	37.3	(58)
Mesoporus iron/aluminum sphere	239	3.0	61.5	(59)
NH_2-Al/SiO_2/Fe_3O_4	122.2	3.0	>40.0	(55)
Iron oxide nano particle	82.2	6.0	3.1	(38)
Goethite + Maghemite	-	4.0	0.9	(44)
Ferrihydrite	178.8	7.0	66.7	This study
Magnetite	123.1	7.0	57.8	This study
Goethite	86.5	7.0	50.5	This study

Note: q means adsorbed amount ($mg.g^{-1}$).

Graphical Abstract